Chemical Science

RSC Publishing

EDGE ARTICLE

View Article Online
View Journal | View Issue

Cite this: *Chem. Sci.*, 2013, **4**, 2483

Stabilizing unstable species through single-site isolation: a catalytically active Ta^V trialkyl in a porous organic polymer†

Kristine K. Tanabe,[a] Nathan A. Siladke,[a] Erin M. Broderick,[a] Takeshi Kobayashi,[b] Jennifer F. Goldston,[bc] Mitchell H. Weston,[d] Omar K. Farha,[d] Joseph T. Hupp,[ad] Marek Pruski,[bc] Elizabeth A. Mader,*[a] Marc J. A. Johnson*[a] and SonBinh T. Nguyen*[ad]

Received 18th December 2012
Accepted 22nd February 2013

DOI: 10.1039/c3sc22268c

www.rsc.org/chemicalscience

A catechol-functionalized porous organic polymer (POP) has been successfully metallated with a Ta^V trialkyl and remains thermally and structurally robust. The resulting POP-supported (catecholato)Ta^V trialkyl sites remain accessible to small molecules and can undergo reactions to yield stable, monomeric complexes that are quite different from those observed with the homogeneous analogues. Using a combination of reactivity studies, high-resolution solid-state NMR spectroscopy, and X-ray absorption spectroscopy (XAS), we are able to precisely determine the functionality and coordination environment of the active (catecholato)Ta^V trialkyl site and its products in reactions with Brønsted acids. Additionally, the Ta-metallated POP was found to have enhanced catalytic activity in the hydrogenation of cyclohexene and toluene relative to a homogeneous analogue.

Introduction

Porous organic polymers (POPs) are highly crosslinked, microporous, amorphous materials that are generally constructed using one or more organic building blocks *via* various carbon–carbon or carbon–heteroatom formations.[1–4] Such POP syntheses include, but are not limited to cross-couplings,[5–7] condensation reactions,[8,9] acetylene- or nitrile-trimerizations,[10–13] and "click" chemistry.[14] In addition to applications in gas storage[15–20] and separations,[21,22] POPs have shown excellent promise as an emerging class of heterogeneous catalysts given their high thermal stability (up to 500 °C) and exceptional chemical robustness to acids, bases, and organic solvents (both polar and non-polar).[14,23–30] Since POPs are composed of strong covalent bonds and are highly crosslinked, they are mechanically robust and can withstand harsh conditions (*e.g.*, high temperature and pressure) that are sometimes employed in catalysis. Another attractive feature of POPs as catalysts is the ability to design them with specific topologies, porosities, and functionalities that affect the overall activity and selectivity of the desired catalytic reaction. Through this approach, it should be possible to produce a POP that can stabilize and isolate catalytically active metal sites within its pores, particularly ones that are quite different from solution (*i.e.*, molecular) analogues in coordination environments.

A number of recent reports have demonstrated the successful preparation of metal-containing catalytically active porous frameworks through pre- and post-synthesis methods.[24,31–35] Cooper and co-workers developed bipyridine-/phenylpyridine-POP systems containing Ir, Ru, and Re species and showed that the Ir version was active for reductive amination.[36] Lin and co-workers produced functionally similar bipyridine-POP systems containing Ir and Ru, and showed that they were active for several catalytic reactions such as Aza-Henry reactions, α-arylation, and aerobic amine-coupling.[12,37] Kaskel and co-workers have also prepared an organometallic framework connected by bis(norbornadiene)rhodium nodes that could catalyze the reduction of cyclohexanone to cyclohexanol.[38]

While the aforementioned developments signify rising interest in the use of metallated POPs as catalysts, POPs with active metal alkyl sites, particularly those of early transition metals, have been scarce despite their wide-spread importance for numerous catalytic processes.[39] To explore this possibility, we set out to integrate a highly reactive Schrock-type Ta^V alkylidene complex ($(^tBuCH_2)_3Ta{=}CH^tBu$)[40] into a POP with the eventual goal of exploring metathetic catalysis inside hydrophobic pore environments, *i.e.*, a step beyond homogeneous[41,42] and surface-grafted silica.[43,44] As a model platform, we chose to work with catPOP $\mathbf{A_2B_1}$, a catechol-containing POP with good

[a]*Chemical Sciences and Engineering Division, Argonne National Laboratory, 9700 S Cass Ave, Lemont, IL, 60439, USA. E-mail: mader@anl.gov; mjjohnson@anl.gov; stn@anl.gov; Fax: +1 630 972-4567; Tel: +1 630 252-3418; +1 630 252-3418; +1 630-252-3548*

[b]*U.S. DOE Ames Laboratory, Ames, IA 50011, USA*

[c]*Department of Chemistry, Iowa State University, Ames, IA 50011, USA*

[d]*Department of Chemistry and International Institute for Nanotechnology, Northwestern University, 2145 Sheridan Road, Evanston, Illinois 60208-3113, USA*

† Electronic supplementary information (ESI) available: Experimental procedures, NMR spectra, additional data, and EXAFS fitting parameters are included. See DOI: 10.1039/c3sc22268c

surface area (~1050 $m^2\ g^{-1}$) and large pores (~12 Å),[45] that can readily accommodate (^{t}BuCH$_2$)$_3$Ta=CH^{t}Bu (~10 Å). The catechol sites in $\mathbf{A_2B_1}$ had been reported to undergo complete metallation with a wide range of Lewis-acidic metal centers such as Mg^{2+}, Mn^{2+}, and Cu^{2+}.[45] Given that Me_2Mg was successfully used as the Mg^{2+} source in this early experiment, (^{t}BuCH$_2$)$_3$Ta=CH^{t}Bu should readily react with the catechol sites and release one or more neopentyl substituents through protonolysis to yield a POP with either (catecholato)Ta(CH$_2{}^t$Bu)$_3$ or (catecholato)(^{t}BuCH$_2$)Ta=CH^{t}Bu sites throughout its pores.

Herein, we present the first report of a POP that complexes a high-oxidation-state, early transition metal alkyl moiety (Scheme 1). By using techniques such as EXAFS and high-resolution solid-state (SS) NMR, we are able to elucidate the coordination environment of the complexed Ta metal centers inside $\mathbf{A_2B_1}$. Additionally, we demonstrate that these active sites remain accessible to small molecules and can undergo reactions to yield stable, monometallic complexes that are quite different from those observed with a homogeneous analogue. Most excitingly, the Ta-supported POP can catalytically hydrogenate cyclohexene and toluene at low catalyst loadings and at much faster rates than its closest soluble molecular counterpart.

Results and discussion

As an initial test of reactivity, $\mathbf{A_2B_1}$ was suspended in a solution of (^{t}BuCH$_2$)$_3$Ta=CH^{t}Bu (1.5 equiv per catechol site) in C_6D_6 and monitored by ^{1}H NMR spectroscopy against an internal ferrocene standard. After 24 h at rt, the concentration of (^{t}BuCH$_2$)$_3$Ta=CH^{t}Bu was noticeably reduced and a significant new resonance due to neopentane appeared at 0.90 ppm (1.13 ± 0.11 equiv per Ta; see Fig. S1 in the ESI†). In contrast, exposing the analogous non-functionalized POP $\mathbf{C_2B_1}$ (**C** = 1,4-diethynylbenzene; as in $\mathbf{A_2B_1}$, the subscripts refer to the ratio of components in the POP, see inset in Scheme 1) to the same (^{t}BuCH$_2$)$_3$Ta=CH^{t}Bu solution affords only a small amount of neopentane (0.29 ± 0.04 equiv per Ta, see Fig. S2 in ESI†). The stock solution of (^{t}BuCH$_2$)$_3$Ta=CH^{t}Bu and ferrocene shows no generation of neopentane after 24 h at rt, strongly suggesting that neopentane is indeed a major product in the reaction between (^{t}BuCH$_2$)$_3$Ta=CH^{t}Bu and the catechol groups of $\mathbf{A_2B_1}$. Based on the observed reaction stoichiometry, we tentatively assign the catPOP-supported Ta^V center to have the (^{t}BuCH$_2$)$_3$-Ta(catecholato) formulation.

Given the promising results from the NMR-scale experiment, $\mathbf{A_2B_1}$ was metallated on a larger scale using a diethyl ether solution of excess (^{t}BuCH$_2$)$_3$Ta=CH^{t}Bu. After allowing the reaction to stir at rt for 22 h, an orange solid was obtained, albeit in >100% yield based on the (^{t}BuCH$_2$)$_3$Ta(catecholato) stoichiometry. This slightly super-stoichiometric yield can be attributed to trapped solvent and residual (^{t}BuCH$_2$)$_3$Ta=CH^{t}Bu within the pores of the framework, as confirmed by the release of (*E*/*Z*)-3,3-dimethyl-1-phenyl-1-butene (~5–10 mol% of the catechol loading) upon treating this solid with benzaldehyde (1 equiv based on the catechol loading).[46] Since the amount of obtained olefin is equivalent to the excess Ta loading, this offered further evidence that the catPOP-supported Ta^V site does not have a neopentylidene substituent and is best described as (^{t}BuCH$_2$)$_3$Ta(catecholato). For convenience, we will henceforth refer to the Ta-metallated catPOP as (^{t}BuCH$_2$)$_3$Ta-$\mathbf{A_2B_1}$, with a stoichiometry of 1 Ta per catechol unit.

ICP-AES (inductively coupled plasma atomic emission spectroscopy) analysis revealed (^{t}BuCH$_2$)$_3$Ta-$\mathbf{A_2B_1}$ to contain 22 wt% Ta^V (theoretical metallation = 24 wt%) (Table S1 in ESI†). The ATR-IR (attenuated total reflectance infrared) spectrum of (^{t}BuCH$_2$)$_3$Ta-$\mathbf{A_2B_1}$ (Fig. 1) corroborated the ICP-AES findings through the complete disappearance of the intense catechol O–H stretch (~3500 cm^{-1}) present in the parent catPOP $\mathbf{A_2B_1}$. In place of the O–H stretch, new C–H vibrational modes associated with the neopentyl groups (both –CH$_3$ and –CH$_2$ moieties) were located around 2800–2900 cm^{-1}, and at 1366 and 1461 cm^{-1}, respectively, consistent with data reported by Basset and co-workers for (^{t}BuCH$_2$)$_3$Ta=CH^{t}Bu grafted on silica.[47] New peaks corresponding to Ta–O stretches were also observed around 600–800 cm^{-1}, supporting our assignment that Ta^V coordinates to catecholate groups within the POP.[48]

^{1}H DP- (direct polarization) and ^{1}H–^{13}C CP (cross-polarization)-MAS (magic angle spinning) NMR analysis of (^{t}BuCH$_2$)$_3$Ta-$\mathbf{A_2B_1}$ provided further evidence that (^{t}BuCH$_2$)$_3$Ta=CH^{t}Bu did indeed form a catecholate complex. The ^{1}H DPMAS spectrum of (^{t}BuCH$_2$)$_3$Ta-$\mathbf{A_2B_1}$ (Fig. 2, top panel) exhibited two main resonances at 7.3 and 1.1 ppm, corresponding to the aromatic C–H protons and the superposition of the –CH$_3$ and –CH$_2$ protons of the neopentyl groups, respectively.[49,50] In contrast, only one

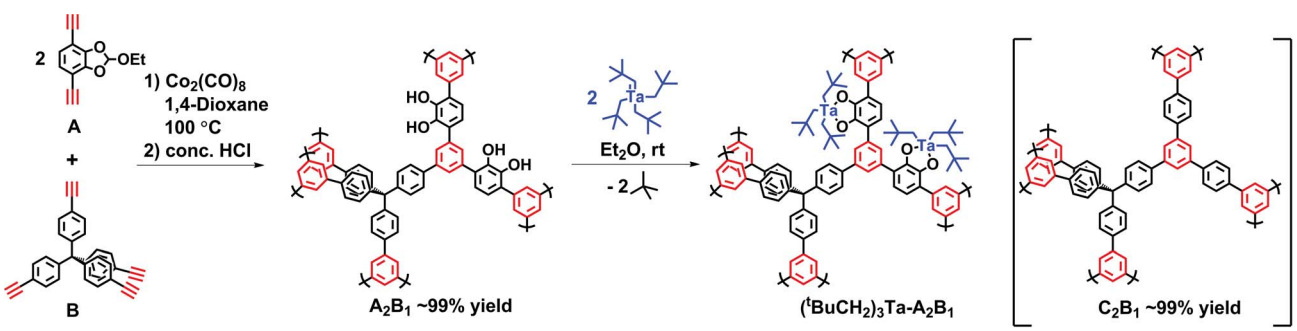

Scheme 1 Synthesis of catPOP $\mathbf{A_2B_1}$ using a cobalt-catalyzed acetylene trimerization strategy and its subsequent metallation with (^{t}BuCH$_2$)$_3$Ta=CH^{t}Bu. Shown on the right hand side is the non-functionalized POP $\mathbf{C_2B_1}$. The structures shown for the POPs are idealized representations.

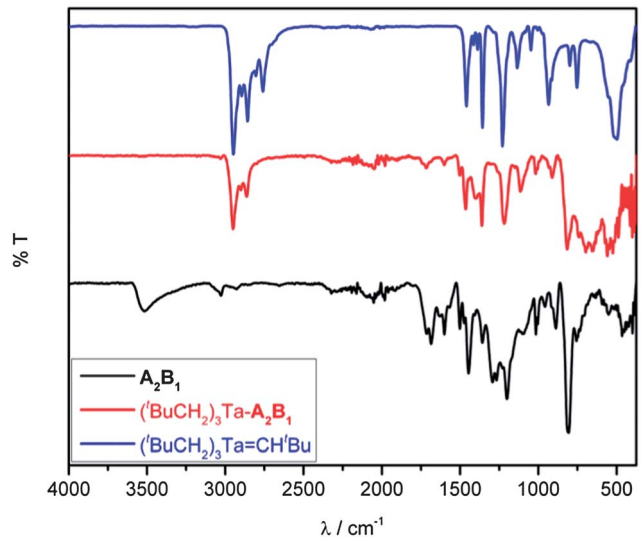

Fig. 1 ATR-IR comparison of (^{t}BuCH$_2$)$_3$Ta=CH^{t}Bu (blue), (^{t}BuCH$_2$)$_3$Ta-**A$_2$B$_1$** (red), and **A$_2$B$_1$** (black).

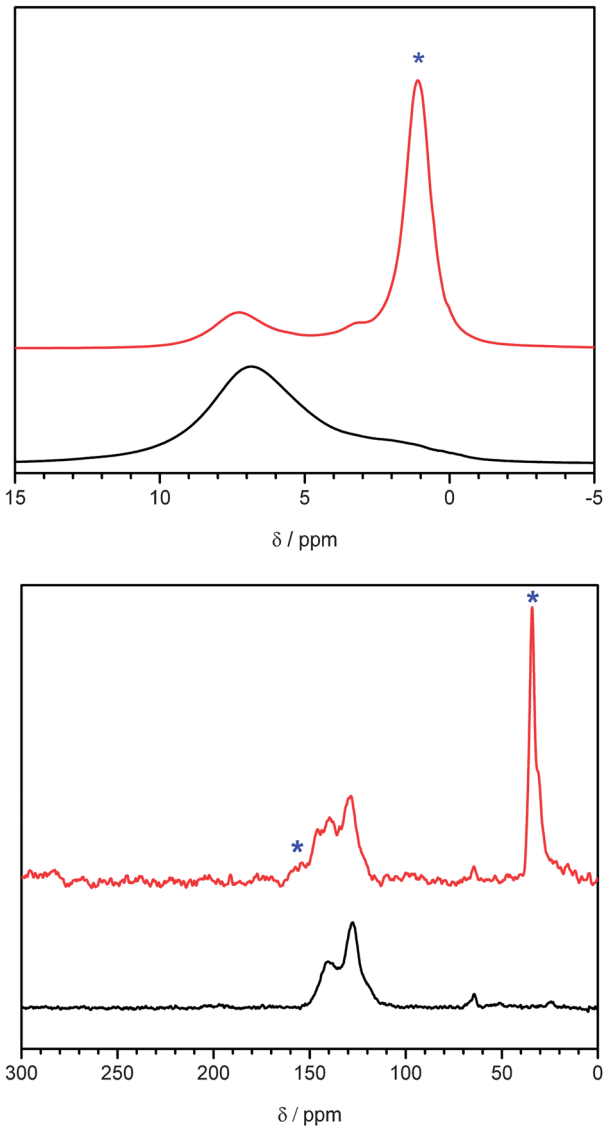

Fig. 2 ^{1}H DPMAS (top) and ^{1}H–^{13}C CPMAS (bottom) NMR spectra of **A$_2$B$_1$** (black) and (^{t}BuCH$_2$)$_3$Ta-**A$_2$B$_1$** (red). The blue asterisks indicate new resonances associated with the newly incorporated Ta moiety.

main resonance at 7.3 ppm was located in the ^{1}H DPMAS spectra of **A$_2$B$_1$**, which corresponded to aromatic C–H protons. The integration ratio of the aromatic protons at 7.3 ppm and the alkyl protons at 1.1 ppm of (^{t}BuCH$_2$)$_3$Ta-**A$_2$B$_1$** were found to be in a 1 : 3.5 ratio, (calc. 1 : 2.5), which is not unreasonable given the trapped (^{t}BuCH$_2$)$_3$Ta=CH^{t}Bu and the resolution of the experiment.

Not surprisingly, the ^{1}H–^{13}C CPMAS spectra of **A$_2$B$_1$** and (^{t}BuCH$_2$)$_3$Ta-**A$_2$B$_1$** (Fig. 2, bottom panel) showed several similarities, including a resonance for the quaternary carbon of the tetraphenylmethane node at 64 ppm and several overlapping resonances between 120–150 ppm for the aromatic carbons. However, several new resonances that are clearly indicative of the Ta^V catecholate complex were detected in the spectrum for (^{t}BuCH$_2$)$_3$Ta-**A$_2$B$_1$**. Notably, a very strong signal for the neopentyl methyl carbons (O–Ta–CH$_2$(C(*C*H$_3$)$_3$)) was found at 34 ppm. Unfortunately, the signal from O–Ta–*C*H$_2$(CH$_3$)$_3$, which is expected around ~100 ppm,[49,50] could not be resolved against the backbone resonances of **A$_2$B$_1$**. A new downfield aromatic resonance at ~157 ppm was also identified and attributed as the newly formed *C*–OTa carbon. This assignment was confirmed by the solution ^{13}C NMR spectrum of the monomeric model complex (^{t}BuCH$_2$)$_3$Ta(3,6-^{t}Bu$_2$cat) (cat = catecholate; see Section S4 in the ESI† for characterization data), which has a similar resonance around ~156 ppm for the *C*–OTa carbon. It is also consistent with the data reported for Ta(cat)$_2$(cat-H)(py),[51] which assigned the *C*–OTa resonance to 159 ppm in solution and 157 ppm in the solid state.

In general, the overall thermal and structural stability of **A$_2$B$_1$** did not appear to be affected by the incorporation of the Ta^V complex. Thermogravimetric analysis (TGA) of (^{t}BuCH$_2$)$_3$Ta-**A$_2$B$_1$** showed two main weight losses around 180 and 480 °C (Fig. S3 in the ESI†), signifying the loss of the three neopentyl groups (~28 wt% calc., 27 wt% observed) and the overall decomposition of the framework, respectively. Gas-sorption analysis of (^{t}BuCH$_2$)$_3$Ta-**A$_2$B$_1$** under N$_2$ at 77 K revealed it to remain quite porous with a BET surface area of 622 ± 10 m^2 g^{-1} (Fig. 3, BET surface area for catPOP = 1000 ± 50 m^2 g^{-1}) despite the presence of large (^{t}BuCH$_2$)$_3$Ta-**A$_2$B$_1$** moieties within at least some of the pores.

Thus far, all of our characterization data for (^{t}BuCH$_2$)$_3$Ta-**A$_2$B$_1$** have indicated the presence of a stable Ta^V alkyl complex bound to catecholate sites. To directly probe the coordination environment around the POP-supported metal center and confirm our initial assignment of the (^{t}BuCH$_2$)$_3$Ta-**A$_2$B$_1$** formulation, we obtained the Ta-L$_{III}$-edge EXAFS spectrum for (^{t}BuCH$_2$)$_3$Ta-**A$_2$B$_1$** (Fig. 4b). As a model, the Ta-L$_{III}$-edge EXAFS spectrum for the molecular compound (^{t}BuCH$_2$)$_3$Ta(3,6-^{t}Bu$_2$cat) (Fig. 4a), which exists as a five-coordinate complex (see below), was also obtained. Examination of the first coordination shell for (^{t}BuCH$_2$)$_3$Ta-**A$_2$B$_1$** shows an average C/O coordination

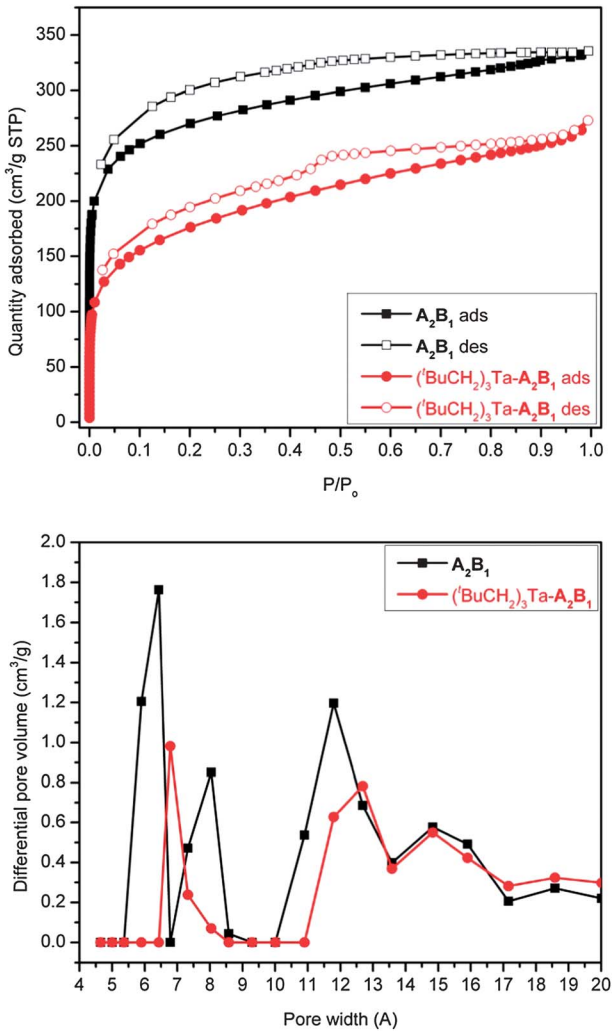

Fig. 3 Full N_2-adsorption isotherm analysis of POPs (top) and the corresponding pore size distribution data using N_2-DFT slit-pore model (bottom).

number of 4.8 ± 0.2 at a mean distance of 2.01 ± 0.02 Å. This is consistent with the fitting of $(^t\text{BuCH}_2)_3\text{Ta}(3,6\text{-}^t\text{Bu}_2\text{cat})$, which has an average C/O coordination number of 5.2 ± 0.3 at a mean distance of 2.01 ± 0.02 Å. The spectrum fits for both $(^t\text{BuCH}_2)_3\text{Ta-}\mathbf{A_2B_1}$ and $(^t\text{BuCH}_2)_3\text{Ta}(3,6\text{-}^t\text{Bu}_2\text{cat})$ correspond well with each other and with an environment comprising two oxygens from the catechol and three carbons from neopentyl groups being directly bound to Ta (average Ta–C = 2.19 ± 0.09 Å, Ta–O = 1.98 ± 0.12 Å).[51–54] Together with the fact that the EXAFS spectrum of $(^t\text{BuCH}_2)_3\text{Ta}{=}\text{CH}^t\text{Bu}$ was quite distinct from $(^t\text{BuCH}_2)_3\text{Ta-}\mathbf{A_2B_1}$ (*cf.* Fig. S19 and S24 in the ESI†), these results support our $(^t\text{BuCH}_2)_3\text{Ta-}\mathbf{A_2B_1}$ formulation for the POP-supported species.

To explore the difference in chemical reactivity of the supported and homogeneous $(^t\text{BuCH}_2)_3\text{Ta}$ catecholate centers, we exposed $(^t\text{BuCH}_2)_3\text{Ta-}\mathbf{A_2B_1}$ and $(^t\text{BuCH}_2)_3\text{Ta}(3,6\text{-}^t\text{Bu}_2\text{cat})$ to MeOH and anhydrous HCl (Scheme 2). As expected, subjecting either Ta species to MeOH results in the complete conversion of the $(^t\text{BuCH}_2)$–Ta segments to MeO–Ta moieties and the corresponding release of neopentane (Fig. S5, S6, and S9 in the ESI†).

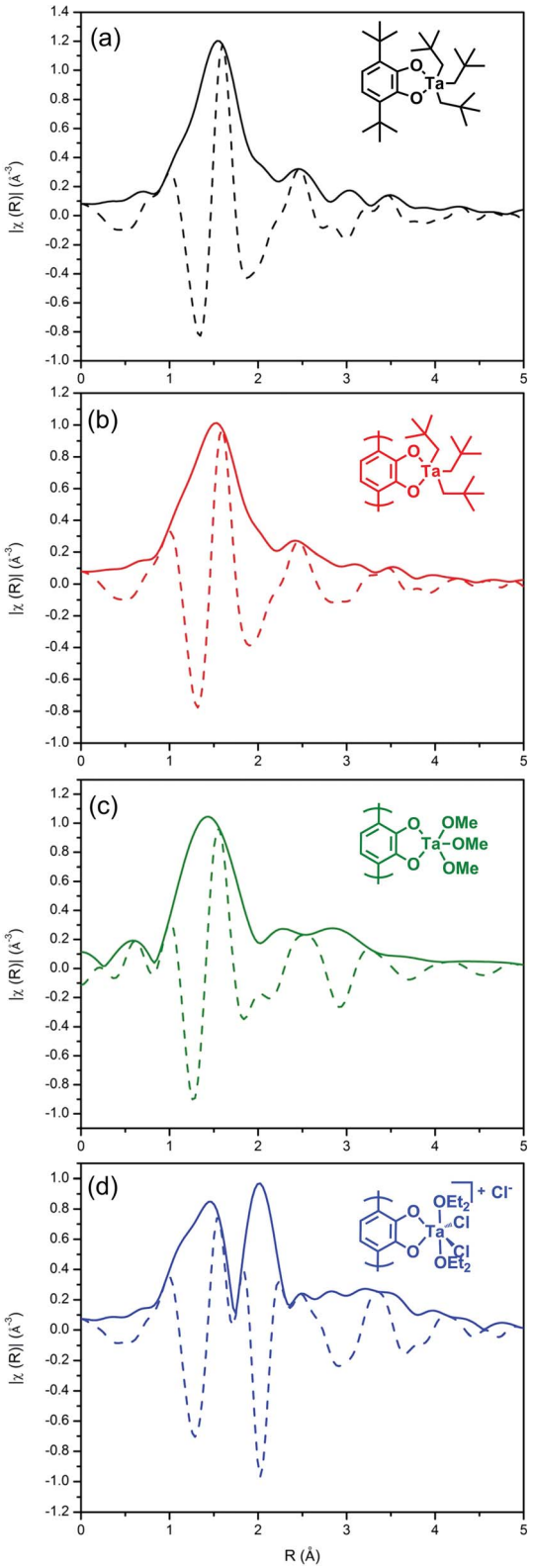

Fig. 4 The Ta L_{III}-edge, k^2-weighted Fourier transform EXAFS spectrum for (a) $(^t\text{BuCH}_2)_3\text{Ta}(3,6\text{-}^t\text{Bu}_2\text{cat})$ (black), (b) $(^t\text{BuCH}_2)_3\text{Ta-}\mathbf{A_2B_1}$ (red), (c) $(\text{MeO})_3\text{Ta-}\mathbf{A_2B_1}$ (green) and (d) $[(\text{Et}_2\text{O})_2\text{Cl}_2\text{Ta-}\mathbf{A_2B_1}]\text{Cl}$ (blue). Magnitudes are shown as solid lines, real components are shown as dotted lines of the same color. Fits and fit parameters are given in the ESI.†

These results are consistent with the TGA data mentioned above and previous protonolysis experiments by the Schrock[40] and Basset[55] groups. However, the homogeneous complex is converted to a six-coordinate MeO-bridged dimer while the Ta centers in (^{t}BuCH$_2$)$_3$Ta-**A$_2$B$_1$** remain five-coordinate, monometallic complexes (Fig. 4c, see Section S6 and the EXAFS analysis in Section S7 of the ESI†). We view this difference as a likely advantage of the isolated pore environment in POP **A$_2$B$_1$**: the supported, coordinatively unsaturated Ta centers cannot come together to form saturated dimers, potentially leaving the supported centers more accessible for catalysis.[55]

Adding a diethyl ether solution of HCl to either (^{t}BuCH$_2$)$_3$Ta-**A$_2$B$_1$** or (^{t}BuCH$_2$)$_3$Ta(3,6-^{t}Bu$_2$cat) leads to complete displacement of (^{t}BuCH$_2$) groups by chlorides, as shown by NMR quantification of the amount of generated neopentane (Fig. S11 in the ESI†). Visually, both (^{t}BuCH$_2$)$_3$Ta-**A$_2$B$_1$** and (^{t}BuCH$_2$)$_3$-Ta(3,6-^{t}Bu$_2$cat) undergo distinct color changes (to black and red, respectively), indicative of reactions taking place. The EXAFS spectrum of the POP-supported product from the [(^{t}BuCH$_2$)$_3$Ta-**A$_2$B$_1$** + HCl] reaction shows a decrease in the total C/O coordination, and the appearance of a second, new Ta coordination shell at much longer distances (Fig. 4d). Fitting this spectrum to a combination of O and Cl scatterers at both distances simultaneously yields a total Ta–O coordination of 4.0 ± 0.3 at an average distance of 1.95 ± 0.02 Å, and a Ta–Cl coordination of 2.0 ± 0.3 at an average distance of 2.35 ± 0.02 Å (average Ta–Cl = 2.34 ± 0.07 Å).[56] In contrast, the analogous reaction of (^{t}BuCH$_2$)$_3$Ta(3,6-^{t}Bu$_2$cat) with HCl in diethyl ether yields a product with total Ta–O coordination of 3.5 ± 0.5 at an average distance of 1.94 ± 0.02 Å, and a Ta–Cl coordination of 2.5 ± 0.5 at an average distance of 2.35 ± 0.02 Å (Table S3 in the ESI†). ^{1}H NMR spectra of this product show coordination of only one diethyl ether molecule per catechol, supporting a monomeric, neutral (Et$_2$O)Cl$_3$Ta(3,6-^{t}Bu$_2$cat) formulation (Fig. S12 in the ESI†). Although we do not know why the Ta chloride species would prefer a cationic environment inside the pores of **A$_2$B$_1$** (Fig. 4c), in contrast to its homogeneous analogue, this observation suggests that constraining metal species inside the pore environment of POP may lead to unique catalytic sites.[57]

The aforementioned experiments suggest that while the reactivity of the neopentyl groups in (^{t}BuCH$_2$)$_3$Ta-**A$_2$B$_1$** is similar to that for the neopentyl groups in (^{t}BuCH$_2$)$_3$Ta(3,6-^{t}Bu$_2$cat), the pore environment of the POP limits the POP-supported Ta coordination environments to monometallic species that are not observed in solution. Most importantly for catalytic applications, the POP environment greatly increases the thermal stability of the (^{t}BuCH$_2$)–Ta bonds and significantly inhibits dimerization. For example, when (^{t}BuCH$_2$)$_3$Ta-**A$_2$B$_1$** was heated at 60 °C in C$_6$D$_6$ over a period of 48 h, the (^{t}BuCH$_2$)$_3$Ta centers were completely stable, as shown by a minimal formation of neopentane (Fig. S8 in ESI†). In contrast, heating (^{t}BuCH$_2$)$_3$-Ta(3,6-^{t}Bu$_2$cat) at 60 °C in C$_6$D$_6$ led to the formation of neopentane in less than 2 h (Fig. S14 in ESI†), presumably *via* α-elimination.

To demonstrate the higher stability and reactivity of (^{t}BuCH$_2$)$_3$Ta-**A$_2$B$_1$** over its homogeneous analogue (^{t}BuCH$_2$)$_3$-Ta(3,6-^{t}Bu$_2$cat), we examined them as hydrogenation catalysts for cyclohexene. At very low catalyst loading (0.5 mol% Ta), (^{t}BuCH$_2$)$_3$Ta-**A$_2$B$_1$** selectively converts cyclohexene to cyclohexane within 2 h under 200 psi H$_2$ and at 60 °C (Fig. 5, see also Fig. S27 in ESI†). In contrast, (^{t}BuCH$_2$)$_3$Ta(3,6-^{t}Bu$_2$cat) and **A$_2$B$_1$** showed little or no conversion, respectively, under identical conditions (Fig. 5, Table S6 in ESI†). Increasing the (^{t}BuCH$_2$)$_3$-Ta(3,6-^{t}Bu$_2$cat) catalyst loading by ten times (to 5 mol%) did improve the conversion to ~99%, suggesting that (^{t}BuCH$_2$)$_3$-Ta(3,6-^{t}Bu$_2$cat) is rather unstable under these conditions and requires a significantly higher loading to achieve the same conversion as (^{t}BuCH$_2$)$_3$Ta-**A$_2$B$_1$**. The substantially higher reactivity observed for (^{t}BuCH$_2$)$_3$Ta-**A$_2$B$_1$** compared to its molecular analogue indirectly suggests that the POP is capable of stabilizing extremely reactive catalytic intermediates, such as (catecholato)TaH$_n$.[42,44,58] Indeed, the higher stability of the Ta-supported POP renders it active for the hydrogenation of toluene at 60 °C, with ~12% conversion after 20 h under 200 psi H$_2$, in stark contrast to the homogeneous analogue, which shows no turnover. Together, these promising results point towards the exciting possibility that highly active POP-based catalysts can be developed for more challenging catalytic targets such as alkane metathesis.

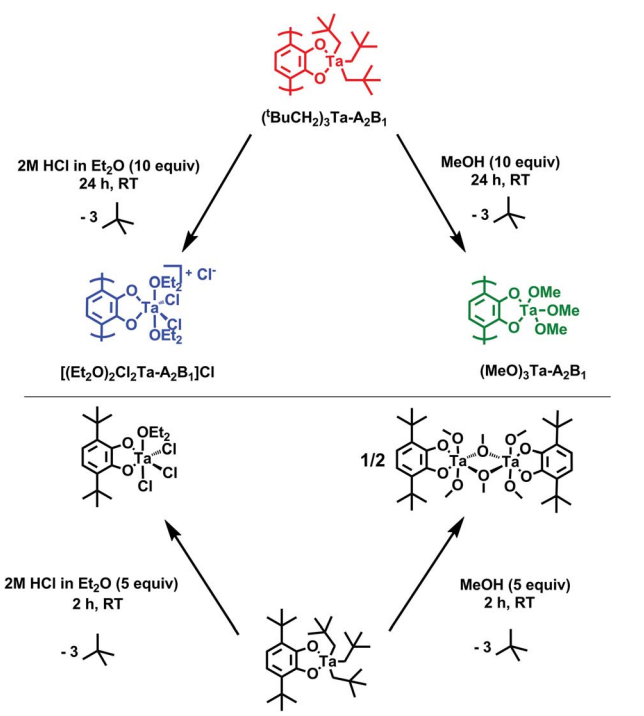

Scheme 2 Summary of the reactivity of (^{t}BuCH$_2$)$_3$Ta-**A$_2$B$_1$** (top) and (^{t}BuCH$_2$)$_3$-Ta(3,6-^{t}Bu$_2$cat) (bottom) with MeOH and HCl.

Conclusions

In summary, we have demonstrated that a POP with well-defined catechol functionalities can react in a controlled manner with a highly reactive organometallic precursor such as (^{t}BuCH$_2$)$_3$Ta=CH^{t}Bu to yield (^{t}BuCH$_2$)$_3$Ta(catecholato) analogues with exceptional thermal stability. Metal loading can

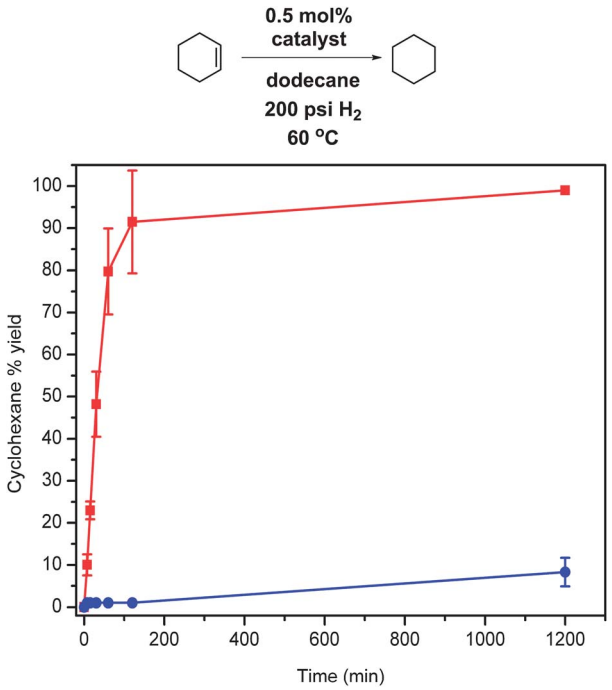

Fig. 5 Yield of cyclohexane from the hydrogenation of cyclohexene (0.5 mol% Ta, 200 psi H_2, 60 °C in dodecane) with $(^tBuCH_2)_3Ta$-$\mathbf{A_2B_1}$ (red) and $(^tBuCH_2)_3$-Ta(3,6-$^tBu_2$cat) (blue) at 0, 7.5, 15, 30, 60, 120, and 1200 min. No other products were observed under these reaction conditions and times (see also Fig. S27 in the ESI†).

be achieved quantitatively and the site isolation allows us to stabilize highly reactive, sterically unencumbered moieties such as (catecholato)Ta(OMe)$_3$ and (catecholato)TaH$_n$. Although POPs are amorphous materials, the catechol-containing pore environments of materials such as $\mathbf{A_2B_1}$ are surprisingly uniform and well-defined, allowing us to apply the powerful combination of solid-state NMR and EXAFS to elucidate the coordination environment of the supported Ta^V species as it undergoes reaction with Brønsted acids. Catalytic studies using the hydrogenation of cyclohexene, a prototypical alkene, as a test reaction indicate that $(^tBuCH_2)_3Ta$-$\mathbf{A_2B_1}$ is indeed an active hydrogenation catalyst. In addition, a comparison of the reactivity between the metallated POP and its closest molecular analogue, $(^tBuCH_2)_3Ta(3,6\text{-}^tBu_2cat)$, clearly demonstrates that POPs designed with specific metal binding sites (in this case the catecholate group) can effectively stabilize highly reactive intermediates. Such capabilities point toward opportunities to develop a new generation of well-defined supported monometallic catalysts whose environment can readily be understood along with their *in situ* reactivity.

Acknowledgements

We thank S. C. Browne, N. David, and L. M. Fenton for synthesizing some of the starting materials used in this work. We thank Dr. M. S. Ferrandon for help with the initial catalysis setup and Dr. S. J. Lopykinski for help with the gas chromatography setup. We thank Drs. J. T. Miller and A. S. Hock for helpful discussions. Work carried out at Argonne National Laboratory was supported by the U.S. Department of Energy, Office of Basic Energy Sciences, under contract DE-AC02-06CH11357. Use of the Advanced Photon Source, a User Facility operated for the U.S. Department of Energy (DOE), Office of Science by Argonne National Laboratory, was also supported by the U.S. DOE under Contract no. DE-AC02-06CH11357. Ames Laboratory's work was supported through the U.S. DOE, Office of Basic Energy Sciences, through Catalysis Science Grant AL-03-380-011 and under Contract W-7405-Eng-82. S. T. N., J. T. H., and O. K. F. additionally acknowledge DTRA (Agreement HDTRA1-10-1-0023) for support.

Notes and references

1 N. B. McKeown and P. M. Budd, *Chem. Soc. Rev.*, 2006, **35**, 675–683.
2 J.-X. Jiang and A. I. Cooper, *Top. Curr. Chem.*, 2010, **293**, 1–33.
3 W. Lu, D. Yuan, D. Zhao, C. I. Schilling, O. Plietzsch, T. Muller, S. Bräse, J. Guenther, J. Blümel, R. Krishna, Z. Li and H.-C. Zhou, *Chem. Mater.*, 2010, **22**, 5964–5972.
4 O. K. Farha, A. M. Spokoyny, B. G. Hauser, Y.-S. Bae, S. E. Brown, R. Q. Snurr, C. A. Mirkin and J. T. Hupp, *Chem. Mater.*, 2009, **21**, 3033–3035.
5 T. Ben, H. Ren, S. Ma, D. Cao, J. Lan, X. Jing, W. Wang, J. Xu, F. Deng, J. M. Simmons, S. Qiu and G. Zhu, *Angew. Chem., Int. Ed.*, 2009, **48**, 9457–9460.
6 A. I. Cooper, *Adv. Mater.*, 2009, **21**, 1291–1295.
7 Y. Yuan, F. Sun, H. Ren, X. Jing, W. Wang, H. Ma, H. Zhao and G. Zhu, *J. Mater. Chem.*, 2011, **21**, 13498–13502.
8 H. M. El-Kaderi, J. R. Hunt, J. L. Mendoza-Cortés, A. P. Côté, R. E. Taylor, M. O'Keeffe and O. M. Yaghi, *Science*, 2007, **316**, 268–272.
9 P. Pandey, A. P. Katsoulidis, I. Eryazici, Y. Wu, M. G. Kanatzidis and S. T. Nguyen, *Chem. Mater.*, 2010, **22**, 4974–4979.
10 W. Wang, H. Ren, F. Sun, K. Cai, H. Ma, J. Du, H. Zhao and G. Zhu, *Dalton Trans.*, 2012, **41**, 3933–3936.
11 S. Yuan, B. Dorney, D. White, S. Kirklin, P. Zapol, L. Yu and D.-J. Liu, *Chem. Commun.*, 2010, **46**, 4547–4549.
12 Z. Xie, C. Wang, K. E. deKrafft and W. Lin, *J. Am. Chem. Soc.*, 2011, **133**, 2056–2059.
13 P. Kuhn, M. Antonietti and A. Thomas, *Angew. Chem., Int. Ed.*, 2008, **47**, 3450–3453.
14 P. Pandey, O. K. Farha, A. M. Spokoyny, C. A. Mirkin, M. G. Kanatzidis, J. T. Hupp and S. T. Nguyen, *J. Mater. Chem.*, 2011, **21**, 1700–1703.
15 S. Yuan, S. Kirklin, B. Dorney, D.-J. Liu and L. Yu, *Macromolecules*, 2009, **42**, 1554–1559.
16 D. Yuan, W. Lu, D. Zhao and H.-C. Zhou, *Adv. Mater.*, 2011, **23**, 3723–3725.
17 M. G. Rabbani and H. M. El-Kaderi, *Chem. Mater.*, 2011, **23**, 1650–1653.
18 S. Yuan, D. White, A. Mason, B. Reprogle, M. S. Ferrandon, L. Yu and D.-J. Liu, *Macromol. Rapid Commun.*, 2012, **33**, 407–413.

19 S. J. Garibay, M. H. Weston, J. E. Mondloch, Y. J. Colón, O. K. Farha, J. T. Hupp and S. T. Nguyen, *CrystEngComm*, 2013, **15**, 1515–1519.
20 B. G. Hauser, O. K. Farha, J. Exley and J. T. Hupp, *Chem. Mater.*, 2013, **25**, 12–16.
21 O. K. Farha, Y.-S. Bae, B. G. Hauser, A. M. Spokoyny, R. Q. Snurr, C. A. Mirkin and J. T. Hupp, *Chem. Commun.*, 2010, **46**, 1056–1058.
22 W. Lu, J. P. Sculley, D. Yuan, R. Krishna, Z. Wei and H.-C. Zhou, *Angew. Chem., Int. Ed.*, 2012, **51**, 7480–7484.
23 H. J. Mackintosh, P. M. Budd and N. B. McKeown, *J. Mater. Chem.*, 2008, **18**, 573–578.
24 P. Kaur, J. T. Hupp and S. T. Nguyen, *ACS Catal.*, 2011, **1**, 819–835.
25 A. M. Shultz, O. K. Farha, J. T. Hupp and S. T. Nguyen, *Chem. Sci.*, 2011, **2**, 686–689.
26 H. C. Cho, H. S. Lee, J. Chun, S. M. Lee, H. J. Kim and S. U. Son, *Chem. Commun.*, 2011, **47**, 917–919.
27 A. Comotti, S. Bracco, M. Mauri, S. Mottadelli, T. Ben, S. Qiu and P. Sozzani, *Angew. Chem., Int. Ed.*, 2012, **51**, 10136–10140.
28 S.-Y. Ding, J. Gao, Q. Wang, Y. Zhang, W.-G. Song, C.-Y. Su and W. Wang, *J. Am. Chem. Soc.*, 2011, **133**, 19816–19822.
29 C. A. Wang, Z. K. Zhang, T. Yue, Y. L. Sun, L. Wang, W. D. Wang, Y. Zhang, C. Liu and W. Wang, *Chem.–Eur. J.*, 2012, **18**, 6718–6723.
30 A. Thomas, *Angew. Chem., Int. Ed.*, 2010, **49**, 8328–8344.
31 J. Lee, O. K. Farha, J. Roberts, K. A. Scheidt, S. T. Nguyen and J. T. Hupp, *Chem. Soc. Rev.*, 2009, **38**, 1450–1459.
32 M. Yoon, R. Srirambalaji and K. Kim, *Chem. Rev.*, 2012, **112**, 1196–1231.
33 R. Palkovits, M. Antonietti, P. Kuhn, A. Thomas and F. Schüth, *Angew. Chem., Int. Ed.*, 2009, **48**, 6909–6912.
34 C. E. Chan-Thaw, A. Villa, P. Katekomol, D. Su, A. Thomas and L. Prati, *Nano Lett.*, 2010, **10**, 537–541.
35 K. Thiel, R. Zehbe, J. Roeser, P. Strauch, S. Enthaler and A. Thomas, *Polym. Chem.*, 2013, **4**, 1848–1856.
36 J.-X. Jiang, C. Wang, A. Laybourn, T. Hasell, R. Clowes, Y. Z. Khimyak, J. Xiao, S. J. Higgins, D. J. Adams and A. I. Cooper, *Angew. Chem., Int. Ed.*, 2011, **50**, 1072–1075.
37 C. Wang, Z. Xie, K. E. DeKrafft and W. Lin, *ACS Appl. Mater. Interfaces*, 2012, **4**, 2288–2294.
38 U. Stoeck, G. Nickerl, U. Burkhardt, I. Senkovska and S. Kaskel, *J. Am. Chem. Soc.*, 2012, **134**, 17335–17337.
39 J.-M. Basset, C. Copéret, D. Soulivong, M. Taoufik and J. Thivolle-Cazat, *Acc. Chem. Res.*, 2010, **43**, 323–334.
40 R. R. Schrock and J. D. Fellmann, *J. Am. Chem. Soc.*, 1978, **100**, 3359–3370.
41 J. S. Yu, B. C. Ankianiec, M. T. Nguyen and I. P. Rothwell, *J. Am. Chem. Soc.*, 1992, **114**, 1927–1929.
42 I. P. Rothwell, *Chem. Commun.*, 1997, 1331–1338.
43 V. Dufand, G. P. Niccolai, J. Thivolle-Cazat and J.-M. Basset, *J. Am. Chem. Soc.*, 1995, **117**, 4288–4294.
44 V. Vidal, A. Théolier, J. Thivolle-Cazat and J.-M. Basset, *Science*, 1997, **276**, 99–102.
45 M. H. Weston, O. K. Farha, B. G. Hauser, J. T. Hupp and S. T. Nguyen, *Chem. Mater.*, 2012, **24**, 1292–1296.
46 R. R. Schrock, *Acc. Chem. Res.*, 1979, **12**, 98–104.
47 V. Polshettiwar, J. Thivolle-Cazat, M. Taoufik, F. Stoffelbach, S. Norsic and J.-M. Basset, *Angew. Chem., Int. Ed.*, 2011, **50**, 2747–2751.
48 J. M. Lopéz-Encarnación, K. K. Tanabe, M. J. A. Johnson and J. Jellinek, 2013, manuscript in submission.
49 H. Ahn and T. J. Marks, *J. Am. Chem. Soc.*, 2002, **124**, 7103–7110.
50 E. Le Roux, M. Chabanas, A. Baudouin, A. de Mallmann, C. Copéret, E. A. Quadrelli, J. Thivolle-Cazat, J.-M. Basset, W. Lukens, A. Lesage, L. Emsley and G. J. Sunley, *J. Am. Chem. Soc.*, 2004, **126**, 13391–13399.
51 T. J. Boyle, L. J. Tribby, T. M. Alam, S. D. Bunge and G. P. Holland, *Polyhedron*, 2005, **24**, 1143–1152.
52 R. E. LaPointe, P. T. Wolczanski and G. D. Van Duyne, *Organometallics*, 1985, **4**, 1810–1818.
53 J. Gavenonis and T. D. Tilley, *Organometallics*, 2002, **21**, 5549–5563.
54 Average bond distances were determined from the Cambridge Structural Database.
55 D. Meunier, A. Piechaczyk, A. de Mallmann and J.-M. Basset, *Angew. Chem., Int. Ed.*, 1999, **38**, 3540–3542.
56 E. Solari, C. Floriani, A. Chiesi-Villa and C. Rizzoli, *J. Chem. Soc., Chem. Commun.*, 1991, 841–843.
57 Y. Chen, E. Callens, E. Abou-Hamad, N. Merle, A. J. P. White, M. Taoufik, C. Copéret, E. Le Roux and J.-M. Basset, *Angew. Chem., Int. Ed.*, 2012, **51**, 11886–11889.
58 V. Vidal, A. Théolier, J. Thivolle-Cazat, J.-M. Basset and J. Corker, *J. Am. Chem. Soc.*, 1996, **118**, 4595–4602.